PHYSICAL REVIEW A VOLUME 11, NUMBER 2 FEBRUARY 1975

Multimode approach to the physics of unstable laser resonators*†

H. Shih and M. O. Scully
Department of Physics and Optical Sciences Center, University of Arizona, Tucson, Arizona 85721

P. V. Avizonis and W. H. Louisell‡
Air Force Weapons Laboratory, Kirtland AFB, New Mexico 87117
(Received 3 December 1973; revised manuscript received 22 July 1974)

In this paper we present a new approach to the problem of unstable laser resonators. We consider a stable resonator in which we insert a thin diverging lens near one mirror. By varying the focal length of the lens, the lens-resonator system can go from stable to unstable. We expand the field in the lens-resonator system in terms of the normal modes of the original stable resonator. The polarization of the lens causes coupling of the stable modes. The present method allows one to introduce the active lasing medium in a natural way, as is shown. The normal modes of the unstable resonator are obtained numerically, along with analytic solutions in certain limiting cases. A physical discussion of the unstable resonator problem is given in terms of a pseudospin picture.

I. INTRODUCTION

Unstable resonators are of practical interest because their large interaction volume is essential for high-power lasers, and because they avoid the problem of damage to semitransparent mirrors.[1] The theoretical description of the mode structure in unstable resonators and the effects of an active lasing medium are problems of current interest.

Using simple geometrical optics arguments, it was demonstrated that the diffraction loss of the lowest-order mode in an unstable resonator is essentially independent of the Fresnel number (or mirror size).[1] It then seemed meaningful to discuss the limiting cases of unstable cavities with infinitely large Fresnel numbers, for which analytical solutions were easily found.[1-4] The unstable modes were simply the analytical continuation of the modes from the stable region.[3] However, they do not converge in the transverse directions and therefore can hardly be regarded as physical solutions.

Another popular approach involves calculating (by numerical means) the "self-consistent fields" in very much the same fashion as in a stable resonator.[1,5,6] The lowest-order modes are shown to be more or less uniformly distributed in the cavity bounded by the mirrors, whereas the modes with higher-order symmetries are shifted more toward the mirror edges in the transverse directions.

In both of the approaches mentioned above, the "modes" have been frequently considered only for "empty cavities." In other words, the effects of the gain[7] and losses of the lasing media on the mode structure has often been neglected.[8]

In the present paper we suggest and investigate a different approach to the problem. Instead of concentrating our attention on the unstable resonator *per se*, in Fig. 1(a), we consider an optically equivalent situation as depicted in Fig. 1(b). In this way we shall investigate the modes of the equivalent unstable resonator as a mixture of the known modes of a properly chosen stable resonator.[9,10] One advantage of this approach is the fact that most laser theories are developed in terms of a mode picture and the effects of the active medium may be included in the present analysis in a natural way. It is perhaps worthwhile to comment at this point that the resulting multimode problem has some elements in common with the multimode studies of Ref. 9.

As discussed above, the introduction of the concave lenses into marginally stable cavities renders them unstable. These lenses serve as a "mode-coupling media"; their inverse focal lengths are related to the coupling parameters. The transition from stable to unstable cavities will be seen to constitute an interesting area of investigation. In particular, we shall see that the mixing of the stable cavity modes shows "anomalous behavior" in the (empty cavity) stable-unstable transition region. We shall show in a later publication that resonant gain of the active medium as well as the diffraction loss associated with the finite mirrors can modify this behavior. These effects are conveniently handled in the present theory.

II. EQUIVALENT RESONATORS

Figure 1(a) depicts the type of unstable optical resonator which we are going to investigate. It has length D' and is bounded at its two ends by mirrors M_1' and M_2' with radius of curvature R_1' and R_2', respectively. Stability of the resonator is

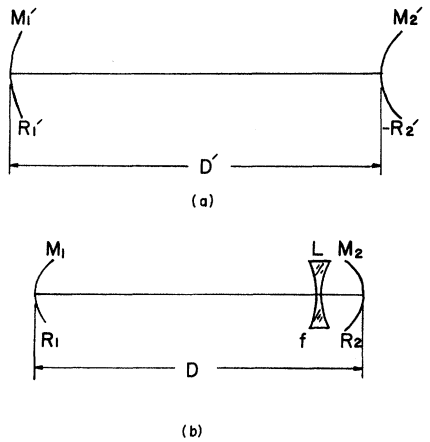

FIG. 1. (a) Schematic diagram for an optical resonator. (b) Resonator with a lens inserted is optically equivalent to the system (a).

characterized by the parameter g' defined as,[10]

$$g' = (1 - D'/R_1')(1 - D'/R_2') . \tag{2.1a}$$

It is unstable if $g' > 1$ or $g' < 0$.

Instead of this resonator, let us consider the equivalent system in Fig. 1(b), which has a concave lens L inserted between the end mirrors M_1 and M_2. Without the lens, the cavity is chosen to be stable, i.e.,

$$0 \leq g = (1 - D/R_1)(1 - D/R_2) \leq 1 . \tag{2.1b}$$

For this resonator the modes are well known.[10]

We will take $R_1 = R_1'$, $D = D'$ and assume that L lies very close to M_2. The combination of L and M is assumed to have an equivalent focal length equal to that of M_2'. This can be realized if we take

$$\frac{1}{f} = \frac{1}{R_2'} - \frac{1}{R_2}, \tag{2.2}$$

where f denotes the focal length of the lens L. Under these conditions, the systems in Figs. 1(a) and 1(b) have the same stability parameter g'. They are both unstable.

To describe the behavior of this lens-resonator system, we shall take the semiclassical approach. The electromagnetic field will be treated classically and its vector character (polarization) will be ignored for simplicity. The field then obeys the following wave equation

$$\left(-\nabla^2 + \frac{1}{c^2}\frac{\partial^2}{\partial t^2}\right) E(\vec{r}, t) = -\mu_0 \left(\frac{\partial}{\partial t}\right)^2 P(\vec{r}, t) .$$

The effect of the electromagnetic field on the atoms in the cavity as well as in the lens is to produce the macroscopic polarizations P_{lase} and P_{lens}. The total polarization P is then

$$P = P_{\text{lens}} + P_{\text{lase}} .$$

The effect of the nonresonant part of the cavity contribution is to change the velocity of light from c to v. To treat the resonant lasing contribution, we can use the simple model of quantum-mechanical two-level atoms interacting with the classical electromagnetic field.[7] The wave equation becomes

$$\left(-\nabla^2 + \frac{1}{v^2}\frac{\partial^2}{\partial t^2}\right) E = -\mu_0 \left(\frac{\partial}{\partial t}\right)^2 (P_{\text{lase}} + P_{\text{lens}}) , \tag{2.3}$$

where

$$P_{\text{lens}} = \epsilon_0 \chi E \quad \text{inside the lens}$$
$$= 0 \qquad \text{otherwise} . \tag{2.4}$$

We expand the field and the total polarization in the "complete orthonormal" set of modes,[11] $\{\mu_\xi(\vec{r})\}$, of the empty stable resonator.[10] Thus,

$$E(\vec{r}, t) = \text{Re}\left(\sum_\xi E_\xi(t)\mu_\xi(\vec{r})\right),$$
$$P(\vec{r}, t) = \text{Re}\left(\sum_\xi P_\xi(t)\mu_\xi(\vec{r})\right) . \tag{2.5}$$

From the orthogonality condition, the paraxial and the slowly varying approximations,[7] the wave equation of (2.3) is reduced to a set of coupled first-order time-dependent equations,

$$\left(\frac{\partial}{\partial t} + i\omega_\xi\right) E_\xi(t) = \tfrac{1}{2} i\omega_\xi v^2 \mu_0 P_\xi(t), \tag{2.6}$$

where

$$\omega_\xi = 2\pi v/\lambda_\xi \equiv v k_\xi .$$

If we further assume that the laser field inside the cavity consists of mixings of high Q modes, the diffraction loss can be incorporated into our equation as phenomenological damping $\Gamma_\xi^{(d)}$:

$$\left(\frac{\partial}{\partial t} + i\omega_\xi(1 - \tfrac{1}{2}\chi_\xi) + \Gamma_\xi^{(d)}\right) E_\xi(t) = \frac{i\omega_\xi}{2} \sum_{\xi' \neq \xi} \{\chi_{\xi\xi'} E_{\xi'}(t) + v^2 \mu_0 P_\xi^{\text{res}}\}, \tag{2.7}$$

where

$$\chi_{\xi\xi'} = (v^2/c^2) \int_{\text{lens}} d^3\vec{r}\, \mu_\xi^*(\vec{r}) \chi \mu_{\xi'}(\vec{r}) \tag{2.8}$$

and

$$\chi_\xi \equiv \chi_{\xi\xi} . \tag{2.9}$$

The main object of the present analysis is to establish the feasibility of handling the unstable resonator problem with the present multimode approach. We see that the effect of the active (gain) medium can be incorporated in a natural way by well-known techniques.[7] The active medium will be treated in a later paper.

III. MODE COUPLING DUE TO LENS

In this section we shall calculate the mode-coupling matrix elements $\chi_{\xi\xi'}$ of (2.8) due to the presence of the lens. We then obtain the coupled equations which will determine the normal modes of the unstable resonator when loss is neglected. We then specialize to a particular resonator configuration which will be extensively studied below. We shall take loss into account in Sec. VI.

We assume mirrors M_1 and M_2 and the lens in Fig. 1(b) are bounded by paraboloidal surfaces so that the system is axially symmetric about the z axis. The normal modes of the stable resonator[10] which we use in (2.8) are ($\xi \equiv q, l, m$)

$$\mu_{qlm}(\vec{r}) = [l!/\pi(l+m)!Dw^2]^{1/2} s^{m/2} L_l^m(s) e^{-s/2} e^{iS}, \tag{3.1}$$

where

$$s \equiv 2r^2/w^2,$$

$$S = -m\phi + k[z - (r^2/2R)] - (2l+m+1)\tan^{-1}\zeta,$$

$$\zeta \equiv 2z/kw_0^2, \tag{3.2}$$

and $L_l^m(s)$ are associated Laguerre polynomials. We also have

$$w^2 = w_0^2(1+\zeta^2), \tag{3.3}$$

which is the beam "size" at ζ in the radial direction. The coordinates are chosen so that $w(\zeta=0) = w_0$. The radius of curvature of the wavefront is

$$R = (kw_0^2/2)[1+\zeta^2]\zeta^{-1}. \tag{3.4}$$

It is planar (infinite) at $\zeta = 0$ where the beam minimum occurs.

Boundary conditions at the mirror require that the wave vectors be restricted to the discrete values

$$k_{qlm} = (\pi/D)[q + 1 + \tfrac{1}{2}(2l+m+1)\theta] \equiv \omega_{qlm}/v, \tag{3.5}$$

where

$$\theta \equiv (2/\pi)\cos^{-1}\{[1-(D/R_1)][1-(D/R_2)]\}^{1/2} \tag{3.6}$$

and q, l, m are integers. For typical resonators, $q \cong 10^6$ while l and m are small integers.

Once k_{qlm} is specified for a given mode, then the minimum beam width, w_0, (qlm), is determined by[10]

$$\tfrac{1}{2}kw_0^2 = \frac{[D(R_1+R_2-D)(R_1-D)(R_2-D)]^{1/2}}{(R_1+R_2-2D)} \equiv L_c(R_1, R_2, D), \tag{3.7}$$

which is the diffraction length for the cavity. Note that this length is the same for all cavity modes. It therefore follows that the radius of curvature of the wavefront (3.4) is mode independent, which allows the boundary conditions on the mirrors to be satisfied for all modes within the paraxial approximation.

By (3.7) and (3.3) we see that the beam size in the transverse direction is mode dependent. However, we see that

$$\frac{1}{w^2_{q',l',m'}} = \frac{1}{w^2_{qlm}}\left(1 + \frac{k_{q'l'm'} - k_{qlm}}{k_{qlm}}\right). \tag{3.8}$$

By (3.5) we see that the mode dependence of w^2 is therefore very weak, since $q \sim 10^6$ for typical resonators.

For a thin lens, its longitudinal dimension is negligible compared with its radius of curvature R_L. We then take, for the lens centered at z_L,

$$\chi(\vec{r}) \cong \chi \quad \text{if } |z - z_L| < r^2/2R_L$$
$$\cong 0 \quad \text{elsewhere}. \tag{3.9}$$

The mode-coupling matrix elements $\chi_{\xi\xi'} \equiv \chi_{q'l'm';qlm}$ in (2.8) are found by using (3.9) and (3.1). Thus, if we let $w^2_{q'l'm'} \cong w^2_{qlm}$, we obtain

$$\chi_{q'l'm';qlm} = \frac{\chi}{D}\delta_{mm'}\left(\frac{l'!}{(l'+m)!}\frac{l!}{(l+m)!}\right)^{1/2} \int_0^\infty ds \int_{z_L - r^2/2R_L}^{z_L + r^2/2R_L} dz$$

$$\times \exp\{-i(\pi/D)[q' - q + (l'-l)\theta]z - 2(l'-l)\tan^{-1}(2z/kw_0^2)\}\, e^{-s} s^m L_{l'}^m(s)\, L_l^m(s). \tag{3.10}$$

We have carried out the ϕ integration and have used (3.5). We have also neglected $r^2/2R$ compared with z, which can be justified on the basis of the paraxial approximation and the factor e^{-s} appearing in the integrand.

We next assume the lens is sufficiently thin that when we carry out the z integration, all z-dependent terms in (3.10) may be evaluated at $z = z_L$. This requires that we let the susceptibility χ and the radius of curvature R_L of the lens both approach infinity but keep their ratio constant. The dioptic power f^{-1} of the lens,

$$f^{-1} \cong \chi/R_L, \tag{3.11}$$

thus remains constant. Then (3.10) becomes

$$\chi_{q'l'm';qlm}=\frac{\chi w_L^2\delta_{mm'}}{2R_L D}\left(\frac{l!}{(l+m)!}\frac{l'}{(l'+m)!}\right)^{1/2}\exp\{-i(\pi/D)[q'-q+(l'-l)\theta]z_L$$
$$-2(l'-l)\tan^{-1}\zeta_L\}\int_0^\infty ds\, e^{-s}s^{m+1}L_{l'}^m(s)L_l^m(s), \tag{3.12}$$

where

$$w_L^2\equiv w_0^2(1+\zeta_L^2). \tag{3.13}$$

If we next use the recursion relation[12]

$$(l+1)L_{l+1}^m(s)-(2l+m+1-s)L_l^m(s)+(l+m)L_{l-1}^m(s)=0, \tag{3.14}$$

together with the orthogonality relations for Laguerre polynomials, (3.12) reduces to

$$\chi_{q'l'm';qlm}=\frac{\chi w_L^2}{2R_L D}\delta_{mm'}\exp[-i(\pi/D)(q'-q)]\{\delta_{ll'}(2l+m+1)-e^{-i\phi_L}\delta_{l',l+1}[(l+1)(l+m+1)]^{1/2}$$
$$-e^{i\phi_L}\delta_{l',l-1}[l(l+m)]^{1/2}\},$$

where

$$\phi_L\equiv\pi z_L\theta/D-2\tan^{-1}(2z_L/kw_0^2). \tag{3.15}$$

We therefore see that modes of different m are not coupled by the lens due to the cylindrical symmetry. Furthermore, only modes whose l values differ by ±1 are coupled. Also, it should be noted that corrections to (3.14) are of order $(k_{q'l'm}-k_{qlm})/k_{qlm}\ll1$.

We next relate the lens susceptibility and radius of curvature R_L to the focal length f. We have from geometrical optics[13] that

$$1/f=-(n_L-1)2/R_L, \tag{3.16}$$

where n_L is the index of refraction of the lens (for a concave lens, $R_L>0$). But

$$n_L=(\epsilon_L)^{1/2}=(1+\chi)^{1/2}\cong1+\tfrac{1}{2}\chi,$$

where ϵ_L is the lens dielectric constant since $\chi<1$. Therefore

$$1/f\cong-\chi/R_L. \tag{3.17}$$

The coupled equations (2.7) now become ($\xi\equiv q,l,m$) (neglecting loss)

$$\left[\frac{\partial}{\partial t}+i\omega_{qlm}\left(1-\frac{\chi w_L^2}{4R_L D}(2l+m+1)\right)\right]E_{qlm}(t)=-i\omega_{qlm}\frac{\chi w_L^2}{4R_L D}\sum_{q'}e^{-i\pi(q'-q)\pi z_L/D}\{e^{-i\phi_L}[(l+1)(l+m+1)]^{1/2}E_{q',l+1,m}(t)$$
$$+e^{i\phi_L}[l(l+m)]^{1/2}E_{q',l-1,m}(t)\}, \tag{3.18}$$

where by (3.5)

$$\omega_{qlm}=vk_{qlm}=\Omega_D[q+1+\tfrac{1}{2}(2l+m+1)\theta],$$
$$\Omega_D\equiv\pi v/D. \tag{3.19}$$

Since modes of different m are uncoupled, we shall consider only the axially symmetric mode for which $m=0$ in the remainder of this paper and shall therefore omit the index m from all future equations for simplicity.

We next note that

$$\omega_{q+1,l}-\omega_{q,l}=\Omega_D,\quad \omega_{q,l+1}-\omega_{q,l}=\Omega_D\theta, \tag{3.20}$$

so that the longitudinal modes are farther apart in frequency than the transverse modes. If we assume that the linewidth γ of the active medium is large compared with the frequency spacing of the transverse modes and narrower than that between different axial modes, i.e.,

$$\Omega_D\gg\gamma\gg\theta\Omega_D, \tag{3.21}$$

then we may neglect the coupling between different longitudinal modes. (It can be shown from a perturbation treatment of the coupled equations that there is very little coupling for modes of different q by the lens.)

We next assume that the lowest-order transverse mode ($l=0,m=0$) with fixed longitudinal mode number q_0 is in exact resonance with the lasing molecules so that

$$\omega_0\equiv\Omega_D(q_0+1+\tfrac{1}{2}\theta)\equiv\omega_{q_0,0}. \tag{3.22a}$$

Also,

$$\omega_{q_0,l}=\omega_0+l\theta\Omega_D. \tag{3.22b}$$

If we then let

$$E_{q_0l}(t)=e^{-i\omega_0 t}A_l(t), \tag{3.23}$$

the coupled equations (3.18) reduce to

$$[-i(d/dt)+l-(4F)^{-1}(2l+1)]A_l=-(4F)^{-1}[e^{-i\phi_L}(l+1)A_{l+1}+e^{i\phi_L}lA_{l-1}], \tag{3.24}$$

where we have introduced the dimensionless time

$$\tau=\Omega_D\theta t \tag{3.25}$$

and the mode-coupling parameter

$$F^{-1}=\frac{\chi w_L^2}{R_L D}\frac{\omega_{q_0,l}}{\Omega_D}\frac{1}{\theta}. \tag{3.26}$$

If we use (3.19) and (3.13), F^{-1} may be written as

$$F^{-1}=\frac{\chi}{R_L}\frac{kw_0^2}{\pi\theta}\left[1+\left(\frac{2z_L}{kw_0^2}\right)^2\right]. \tag{3.27}$$

From this and (3.7), we see that F^{-1} is mode independent. Also by (3.13) and (3.19), (3.26) may be written as

$$F^{-1}\Omega_D\theta=\frac{\chi}{R_L}\frac{w_0^2}{D}\left[1+\left(\frac{2z_L}{kw_0^2}\right)^2\right]\times\Omega_D\left[q_0+1+(l+\tfrac{1}{2})\theta\right]. \tag{3.28}$$

In the remainder of this paper we shall restrict ourselves for simplicity to mirrors such that

$$R_1\to\infty \quad \text{(planar)}, \tag{3.29}$$

$$R_2\gg D.$$

From (2.1b), we have for this case that

$$g=1-D/R_2\approx 1, \tag{3.30}$$

so the resonator without the lens is near being unstable.

From (3.29) and (3.6), we see for this case that

$$\theta\cong(2/\pi)(D/R_2)^{1/2}\ll 1. \tag{3.31}$$

Also by (3.7) we see that

$$kw_0^2/2\equiv L_c\cong(DR_2)^{1/2}. \tag{3.32}$$

By (3.31), (3.32), and (3.27) it follows that

$$F^{-1}\cong(\chi/R_L)R_2(1+z_L^2/DR_2). \tag{3.33}$$

However, the lens is located near M_2, so that $z_L\cong D$, and by (3.29) it follows that

$$F^{-1}\cong(\chi/R_L)R_2. \tag{3.34}$$

By a similar argument, since $q_0\approx 10^6$, it follows from (3.28) that

$$F^{-1}\Omega_D\theta\cong 2v(\chi/R_L)(R_2/D)^{1/2}. \tag{3.35}$$

Also, by (3.15) with $z_L\cong D$, it follows that

$$\phi_L=\pi z_L\theta/D-2\tan^{-1}(2z_L/kw_0^2)\ll 1 \tag{3.36}$$

so $e^{\pm i\phi_L}\cong 1$.

If we use (3.31), the resonant frequency (3.22) reduces to

$$\omega_0\cong\Omega_D(q_0+1). \tag{3.37}$$

By (2.1), (2.2), (3.17), and (3.34), the stability parameter for the unstable resonator is

$$g'=1-(D/R_2)(1-F^{-1}). \tag{3.38}$$

Therefore,

$$\left.\begin{array}{l}0<F<1 \quad \text{(unstable)},\\ F>1\\ <0\end{array}\right\}\ \text{(stable)}. \tag{3.39}$$

The coupled equations (3.24) thus reduce to

$$\left(-i\frac{d}{d\tau}+l-(4F)^{-1}(2l+1)\right)A_l=-(4F)^{-1}\{(l+1)A_{l+1}+lA_{l-1}\}, \tag{3.40}$$

where F^{-1} is given by (3.34). The field over the lens, by (2.5), (3.23), (3.1), and (3.2), becomes

$$E_L(r,t)=e^{-i\omega_0 t}\sum_{l=0}^{\infty}A_l(t)\phi_l(s), \tag{3.41}$$

where

$$\phi_l(s)\equiv e^{-s/2}L_l(s), \quad s=2r^2/w_0^2. \tag{3.42}$$

The constants have been incorporated into the A_l. It should be noted that the case we study is that of a "short" cavity, but this restriction is by no means necessary.

IV. NORMAL MODES FOR LOSSLESS UNSTABLE RESONATOR

We neglect diffraction loss and look for solutions of (3.40) of the form

$$A_l(t)=e^{-i\lambda\tau}B_l=e^{-i\lambda\Omega_D\theta t}B_l, \tag{4.1}$$

where the B_l are time independent. Then (3.40) reduces to the eigenvalue equation

$$\sum_{l'}\{(-\lambda+l')\delta_{l'l}+(4F)^{-1}[-(2l'+1)\delta_{l'l}+l'\delta_{l',l+1}+(l'+1)\delta_{l',l-1}]\}B_{l'}=0. \tag{4.2}$$

Since the matrix is Hermitian, the eigenvalues are real. If we let λ^k be the kth eigenvalue which we order in increasing values of λ, and B_l^k be the kth eigenvector, then the field across the lens by (3.41) and (4.1) is for mode k

$$E_L^k(r,t)=e^{-i\Omega_k t}\sum_{l=0}^{\infty}B_l^k\phi_l(s)\equiv e^{-i\Omega_k t}U_k(r), \tag{4.3}$$

where

$$\Omega_k \cong \Omega_D(q_0 + 1 + \theta\lambda^k) \tag{4.4}$$

are the eigenfrequencies.

There are two limiting cases for which the eigenvalue problem and field distribution over the lens may be solved exactly. Although these cases have limited physical significance, they provide some useful insight into the behavior of the unstable resonator modes.

Case 1: $F^{-1} \to 0$ *(lens removed).* (4.5)

This corresponds to the removal of the lens ($\chi \to 0$) as may be seen from (3.34). From (4.2) it follows that

$$\lambda^k = l, \tag{4.6}$$

and by (4.4), the eigenfrequencies are

$$\Omega_k = \Omega_D[q_0 + 1 + \theta l] = \omega_{q_0 l}, \tag{4.7}$$

which are the original stable-resonator normal-mode frequencies as expected.

Case 2: $F^{-1} \gg 1$ *(geometrical optics limit).*

For this case we have by (3.34) and (3.17)

$$F^{-1} = (-f)^{-1}R_2, \tag{4.8}$$

and we may realize it by keeping $(-f)$ fixed and letting $R_2 \gg (-f)$. Thus mirror M_2 is also approximately planar in this case. In this limit, we may neglect l compared with $(4F)^{-1}(2l+1)$ in (3.40) so we have

$$-i\frac{dA_l}{d\tilde{\tau}} = (2l+1)A_l - (l+1)A_{l+1} - lA_{l-1}, \tag{4.9}$$

where we have let

$$\tilde{\tau} = (4F)^{-1}\tau = (4F)^{-1}\Omega_D\theta t \cong 2v(\chi/R_L)(R_2/D)^{1/2}t \tag{4.10}$$

and we have used (3.35).

A solution of (4.9) is

$$A_l(t) = \int_0^\infty ds'\, e^{is'\tilde{\tau}}\phi_l(s')G(s'), \tag{4.11}$$

where $G(s)$ is an arbitrary function of s. To show this we substitute (4.11) into (4.9) and use the recursion relation (3.14) with $m = 0$. If we use (4.11) in (3.41), we obtain the field distribution across the lens

$$\begin{aligned} E_L(r,t) &= e^{-i\omega_0 t}\int_0^\infty ds'\, e^{is'\tilde{\tau}}G(s')\sum_{l=0}^{\infty}\phi_l(s')\phi_l(s) \\ &= e^{-i\omega_0 t}\int_0^\infty ds'\, e^{is'\tilde{\tau}}G(s')\delta(s'-s) \\ &= G(r)\exp\{-i[\omega_0 - s(4F)^{-1}\Omega_D\theta]t\}. \end{aligned} \tag{4.12}$$

We have used the completeness relation for Laguerre polynomials and (4.10). If we use (3.42), (3.35), and (3.32), this may be written as

$$E_L(r,t) = G(r)e^{-i\omega_0[1 - r^2/(-2fD)]t}. \tag{4.13}$$

In order to relate this to normal modes, we write it as

$$E_L(r,t) = \int_0^\infty dr'\, G(r')E_L^{r'}(r,t), \tag{4.14}$$

where

$$E_L^{r'}(r,t) = e^{-i\Omega_{r'}t}\delta(r'-r) \tag{4.15}$$

and

$$\Omega_{r'} = \omega_0[1 - r'^2/(-2fD)]. \tag{4.16}$$

The modes $E_L^{r'}(r,t)$ have a simple geometrical-optics interpretation. They represent light rays parallel to the z axis bouncing back and forth between two plane-parallel mirrors, since in our result we may let $F^{-1} \to \infty$. The variation in frequency $\omega_0[1 - r^2/(-2fD)]$ in the radial direction is the result of small increases in the optical path due to the presence of the concave lens whose thickness is proportional to r^2. The frequency is downshifted for concave lens ($-2f > 0$) and upshifted for convex ($-2f < 0$).

These modes obviously do not represent physical solutions in real unstable resonators since by (4.15) they have zero radial width, whereas it is known experimentally that the radial width in unstable resonators is very large. They arose because we neglected the l term. If one studies the derivation of (3.40), it arose from the term $\omega_{q_0 l} - \omega_0 = l\Omega_D\theta$, which is the transverse mode frequency. When we neglect it, we are assuming complete degeneracy in the transverse modes. This term is necessary in order to take into account transverse frequency shifts to give a finite beam width. This point will be discussed again quantitatively in Sec. VIII when we obtain asymptotic solutions when $l \to \infty$ and then let $F^{-1} \to \infty$ and obtain physically meaningful solutions. This points up the care that must be exercised in the order in which the limits $l \to \infty$ and $F^{-1} \to \infty$ are taken.

V. NUMERICAL RESULTS FOR LOSSLESS UNSTABLE RESONATORS

The normal-mode frequencies Ω_k and the coefficients B_l^k in (4.3) and (4.4) are found by solving the eigenvalue problem (4.2) by computer. We therefore must restrict l to a finite number of modes, l_m. The choice of l_m depends on how fast the series in (4.3) converges.

In Fig. 2 we show the numerically computed eigenvalues λ from (4.2) with ten modes coupled, i.e., $l_m = 10$. They are plotted as a function of F^{-1}.

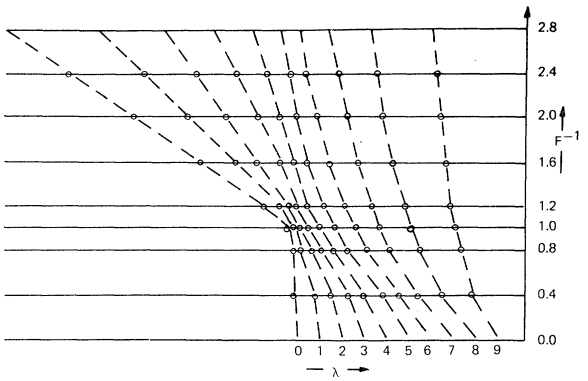

FIG. 2. Dependence of the eigenvalues λ on the stability parameter F^{-1}: Ten modes are coupled, i.e., $l_m = 10$, in the numerical calculations for $F^{-1} = 0$, 0.4, 0.8, 1.0, 1.2, 1.6, 2, 2.4, 2.8. Special attention is called to the transition region $F^{-1} \sim 1$.

For each value of F^{-1}, there are ten eigenvalues. The modes are stable for $0 \leq F^{-1} \leq 1$ and unstable for $F^{-1} > 1$. In order better to display the results in the strongly unstable limit, $F^{-1} \to \infty$, the same results are shown in Fig. 3 with the vertical scale changed to F. The horizontal axis is measured in units of F^{-1}.

We see that all the eigenvalues λ^k are positive for stable resonators, whereas they all become negative in the strongly unstable ($F \to 0$) region. Some eigenvalues (beginning with the lowest) start becoming negative in the transition region, $F^{-1} = 1$, as seen in Fig. 2.

The singular feature of the transition region is more evident if we look at the field distribution for the new eigenmodes. Figure 4 illustrates how the lowest-order mode (smallest λ^k), which is pure Gaussian for $F^{-1} = 0$ (lens absent), changes near the transition region $F^{-1} = 1$. The field amplitude is plotted as a function of the normalized radius,

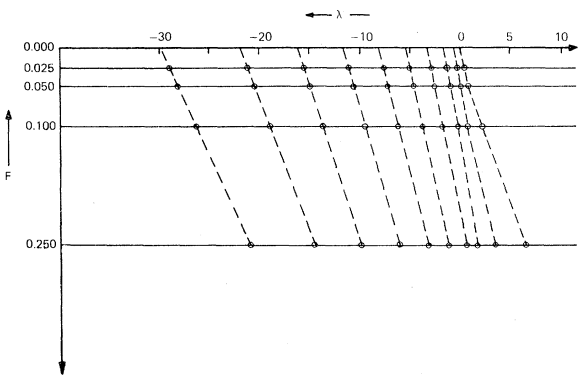

FIG. 3. Behaviors of the eigenvalues λ in the severely unstable region $F^{-1} \to \infty$: The vertical scale here is F, the inverse of that in Fig. 2.

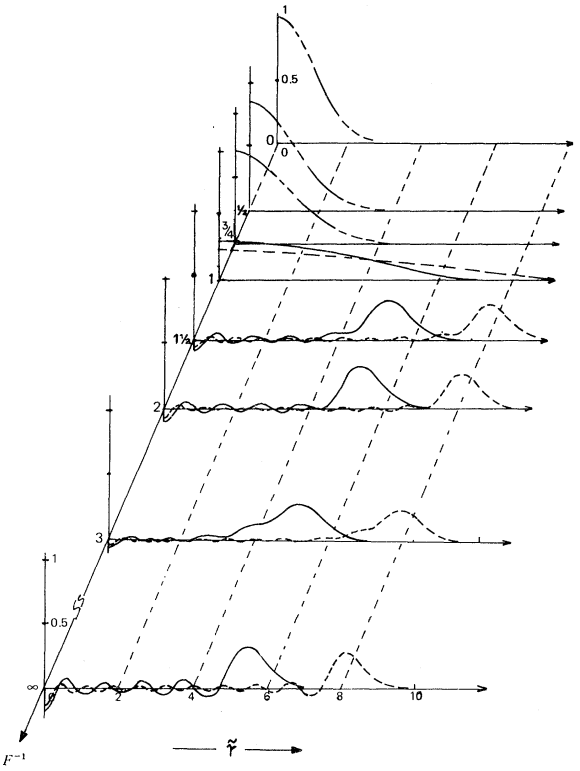

FIG. 4. Mode pattern for the lowest eigenfrequency mode: Vertical axis is the field amplitude $U_0(r)$, horizontal axis denotes the normalized radial distance $\tilde{r} = \sqrt{2}r/w_0$, and the third dimension indicates the stability parameter F^{-1}. Solid curves, $l_m = 10$; dashed curves, $l_m = 20$. Abrupt changes in mode pattern near the transition $F^{-1} = 1$ is observed.

$\tilde{r} = \sqrt{2}r/w_0$. The solid curves are plotted for $l_m = 10$ and the dashed curves for $l_m = 20$.

We observe that, whereas the mode is essentially confined near the axis of the resonator, i.e., near $r = 0$, for $F^{-1} < 1$, it flattens out as we approach the marginally unstable case $F^{-1} = 1$. The only reason the field pattern stabilizes as $F^{-1} \to \infty$ and that it peaks about a finite r is that we have taken a finite number of modes. From Fig. 2, we see that it peaks at a bigger radius for $l_m = 20$ than for $l_m = 10$. In the limit $l_m \to \infty$, the mode will no longer be confined to any finite region in an unstable resonator. This is just what one would expect from simple geometric optics.

To demonstrate further the effect of finite l_m on the eigenvalues, λ^k, we plot in Fig. 5 the eigenvalue variation as a function of l_m for the limiting case $F^{-1} \to \infty$. As l_m increases by unity, the additional eigenvalue which appears is always more negative than the last and as $l_m \to \infty$, the last eigenvalue approaches negative infinity. The first one to appear when $l_m = 1$ approaches zero as $l_m \to \infty$.

Also, the spacing between the eigenvalues diminish as $l_m \to \infty$.

VI. EFFECT OF FINITE MIRROR SIZE

So far we have neglected the finite transverse dimensions of the resonator which accounts for large diffraction loss in the unstable resonator. We can account for the finite mirror size by the artifice of assuming that the lens contains absorbing molecules, mainly in their ground state, which are uniformly distributed. Since the lens thickness varies quadratically with radius, the loss increases quadratically with radius if we assume χ is constant, but complex, over the lens:

$$\chi = \chi' + i\chi'' \equiv \chi'(1 + i\Gamma) . \tag{6.1}$$

The coupled equations (3.40) then become

$$\left(-i\frac{d}{d\tau} + l - (4F)^{-1}(1+i\Gamma)(2l+1)\right)A_l = -(4F)^{-1}(1+i\Gamma)[(l+1)A_{l+1} + lA_{l-1}] , \tag{6.2}$$

where now by (3.34)

$$F^{-1} \cong (\chi'/R_L)R_2 . \tag{6.3}$$

The loss is seen not only to cause each mode to decay but also to affect their mixing.

This model replaces the sharp edges by tapered edges. The finite size of resonators is usually characterized by a Fresnel number[14]

$$N_F = a_{\text{eff}}^2/\lambda_0 D , \tag{6.4}$$

where a_{eff} is the effective radius of the mirrors and λ_0 is the fundamental mode wavelength. We would like to relate a_{eff} to our model. We shall use a plausibility argument based on geometrical optics.

If we again consider the case $F^{-1} \gg 1$ and omit the lone l term in (6.2), we see that the solution found in (4.7)–(4.17) is still valid if we replace F^{-1} by $F^{-1}(1+i\Gamma)$ so that

$$E_L(r,t) \sim e^{-i\omega_0 t[1 - r^2/(-2fD)] - t/\tau_d(r)} , \tag{6.5}$$

where

$$1/\tau_d(r) = [\omega_0 r^2/(-2fD)]\Gamma . \tag{6.6}$$

As we saw earlier, this solution corresponds to a light ray traveling parallel to the axis and a distance r from it. The effect of the lens now not only causes a frequency shift, but also introduces a decay due to the presence of loss.

The effective radius is now defined as the maximum radius beyond which the decay time is shorter than the time it takes the light ray to go one round trip within the cavity, i.e.,

$$\tau_d(a_{\text{eff}}) = 2D/v . \tag{6.7}$$

From (6.6) it follows that

$$k_0 a_{\text{eff}}^2 \Gamma/(-f) = 1 , \tag{6.8}$$

where

$$k_0 = \omega_0/v = 2\pi/\lambda_0 . \tag{6.9}$$

If we use (6.4), we have the relation

$$\Gamma = (-f)/2\pi N_F D = (F/N_F)(R_2/2\pi D) . \tag{6.10}$$

Obviously, the limit of large Fresnel number ($N_F \to \infty$) and/or strong coupling ($F \to 0$) will correspond to the small-loss limit ($\Gamma \to 0$).

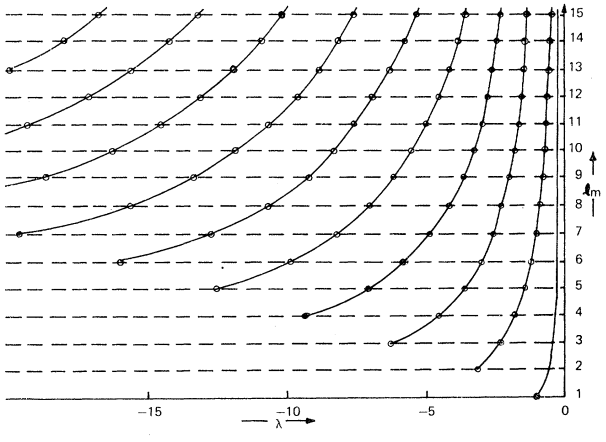

FIG. 5. Eigenvalues in the limit $F^{-1} \to \infty$: The effects of the finite number l_m taken in the numerical calculation is shown here with the vertical axis denoting the changing values of l_m.

VII. NUMERICAL RESULTS FOR LOSSY CASE

The eigenvalue problem (4.2) is modified so that $(4F)^{-1} \to (4F)^{-1}(1+i\Gamma)$ and the eigenvalues λ^k will be complex when loss is included. We have obtained numerical solutions by diagonalizing the matrix in (4.2) with loss included.

In Figs. 6(a)–6(j), real and imaginary parts of the eigenvalues are plotted along the horizontal and vertical axes, respectively. In each plane corresponding to fixed values of Γ and F, the circles indicate the eigenvalues when $l_m = 10$, the triangles when $l_m = 20$, and the squares when $l_m = 40$.

The weak coupling limit, $F^{-1} \to 0$, are shown in Fig. 6(a). By inspection, one finds that in this case

$$\lambda^k \cong k - i\Gamma(2k+1) + \cdots . \tag{7.1}$$

Figs. 6(b)–6(d) are for the marginally stable case of $F^{-1} = 1$, while Figs. 6(e)–6(h) are for the unstable case with $F^{-1} = 2$. For sufficiently large

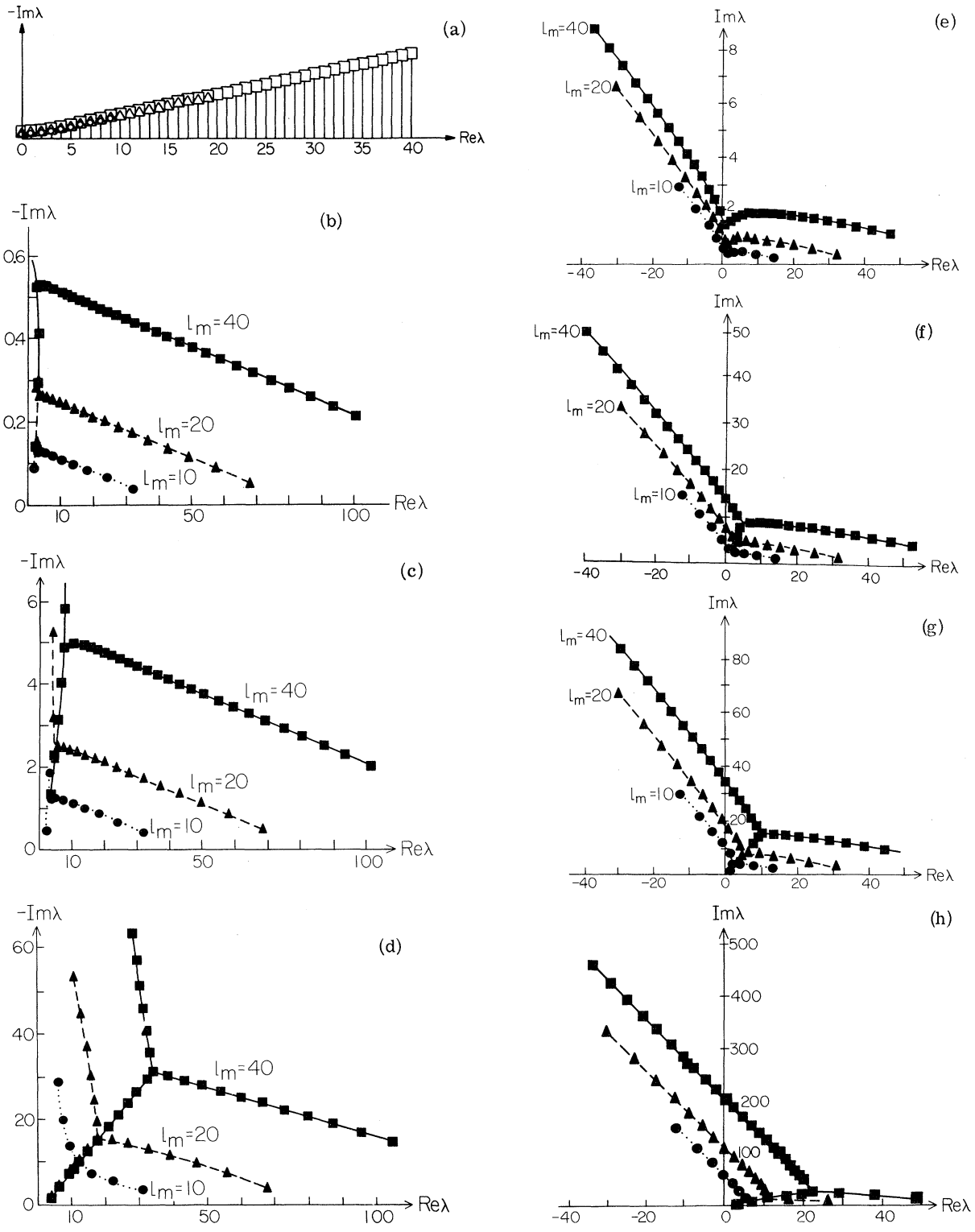

FIG. 6. Effects of the diffractional loss on the eigenvalues λ: The horizontal and vertical axes denote, respectively, the real and imaginary parts of the complex eigenvalues λ. The numerical results are shown as circles, $l_m=10$; triangles, $l_m=20$; squares, $l_m=40$. (a) Stable region with weak coupling $F^{-1}\ll 1$, $\Gamma=0.1$. (b)–(d) Marginal case $F^{-1}=1$: (b) $\Gamma=10^{-2}$, (c) $\Gamma=10^{-1}$, (d) $\Gamma=1$. (e)–(h) Case in the unstable region $F^{-1}=2$: (e) $\Gamma=0.1$, (f) $\Gamma=0.5$, (g) $\Gamma=1$, (h) $\Gamma=5$.

Γ, there are two types of eigenvalues.[15] Type-I is independent of l_m as seen by the fact that circles, triangles, and squares coincide. They have relatively small real and imaginary parts and thus lie close to the origin. On the other hand, type-II eigenvalues depend very strongly on l_m. They tend to have large values of either the real and/or imaginary parts as l_m increases.

Field distributions as a function of r for each λ^k are evaluated according to (4.3). The lowest- as well as the next-to-lowest-order mode of type I are plotted in Figs. 7 and 8, respectively. (The modes are ordered here according to the modulus of their eigenvalues, from small to large.) The vertical axis denotes the field amplitude, $|U_k(r)|$, whereas the abscissa is $\tilde{r} = \sqrt{2}r/w_0$. The results for $l_m = 10$ and 20 are indicated by solid and dashed lines, respectively. They are virtually indistinguishable except for small Γ. This case will be discussed extensively later.

The amplitude dependence on r for the lowest-order modes is Gaussian-like. The width narrows and thus it peaks more toward the axis $r = 0$ as Γ increases. Similar behavior also occurs for the next-to-lowest-order modes, although the amplitude has two peaks rather than just one.

The fact that these type-I modes are virtually the same for $l_m = 10$ and 20 is also clearly illustrated in Figs. 9 and 10. The complex vectors B_l^0 and B_l^1 are shown for the lowest- and the next-to-lowest-order

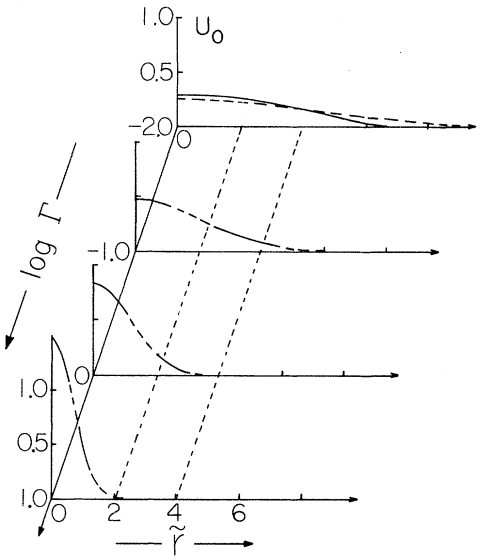

FIG. 7. Lowest-order mode patterns in the marginal case $F^{-1} = 1$: The field amplitudes, $U_0(r)$, are shown for various loss parameters, $\Gamma = 10^{-2}$, 10^{-1}, 1, 10. Solid curves, $l_m = 10$; dashed curves, $l_m = 20$. Except for the case $\Gamma = 0$, the results for $l_m = 10$ and 20 are almost indistinguishable here.

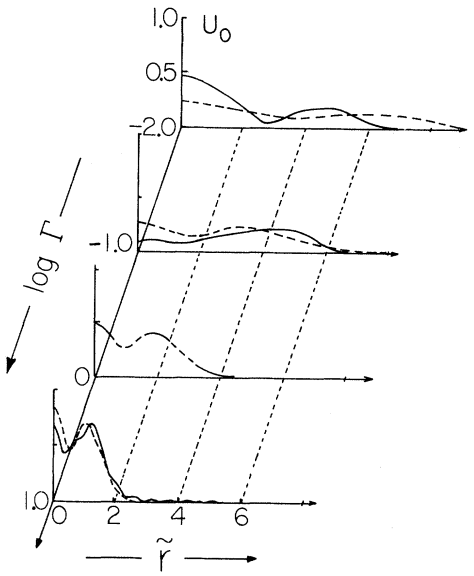

FIG. 8. Field patterns for the next to the lowest-order mode in the marginal case $F^{-1} = 1$. Solid lines, $l_m = 10$; dashed lines, $l_m = 20$.

eigensolutions, respectively. Their amplitude decays almost exponentially for large values of l, and contributions from modes with l greater than 10 are negligible. Furthermore, the angle between successive complex vectors B_l's are almost constant. For the particular case chosen in Figs. 9 and 10 ($F^{-1} = 1$ and $\Gamma = 1$), these angles are almost all equal to $\frac{1}{2}\pi$.

A satisfactory explanation of this observed be-

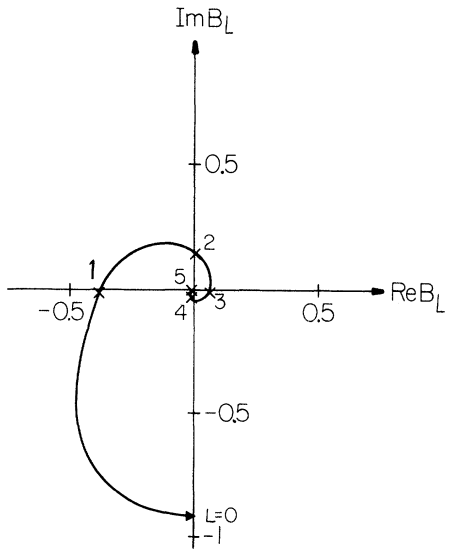

FIG. 9. Components B_l^0 for the lowest mode are shown in the complex plane.

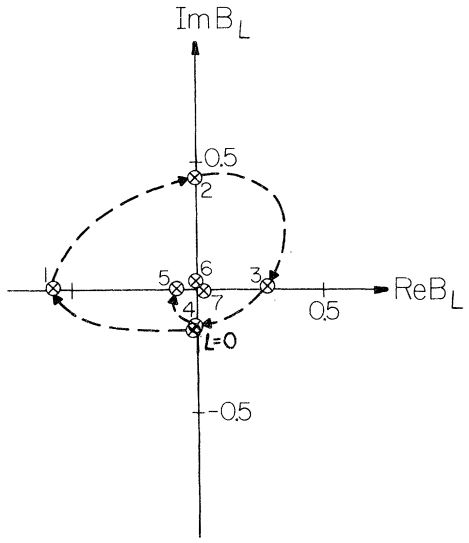

FIG. 10. Components B_l^1 for the next to the lowest-order mode are shown in the complex B plane.

havior will not be attempted until analytic solutions are obtained in Sec. VIII.

To compare the field distributions of the type-II modes with those in Figs. 7 and 8, we also show the results for the two modes with the highest loss (denoted by HL) and the highest frequency (denoted by HF) in Figs. 11 and 12, respectively. As expected, the high-loss modes are sharply peaked and far away from the axis $r=0$, while the high-frequency (low-loss) modes are sharply peaked and close to the axis. The limitation is only due to the finite number l_m of modes that are taken into account in the numerical calculation. This trend is clearly brought out by these figures as l_m increases from 10 to 20.

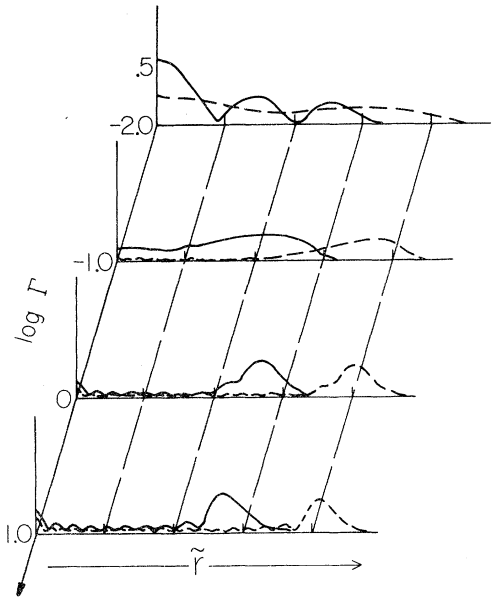

FIG. 11. Mode patterns for the type-II HL mode (with the highest loss) in the marginal case $F^{-1}=1$: Field amplitudes are plotted for various losses; $\Gamma=10^{-2}$, 10^{-1}, 1. Solid curves, $l_m=10$; dashed curves, $l_m=20$.

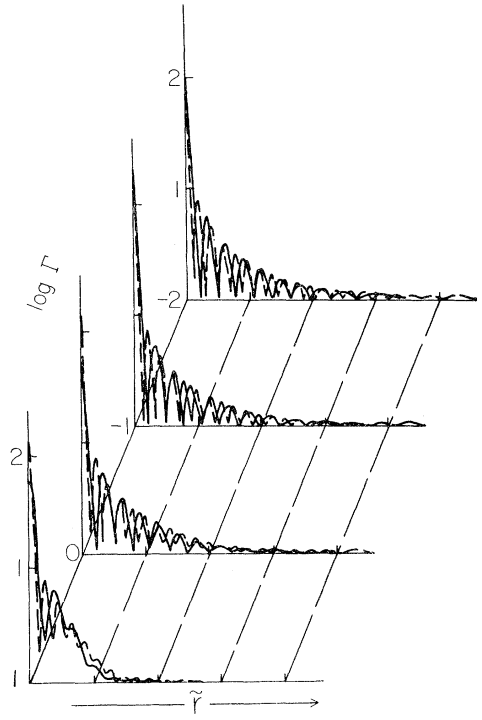

FIG. 12. Mode patterns for the type-II HF mode (with the highest frequency) in the marginal case $F^{-1}=1$.

In contrast to Figs. 9 and 10, the fact that type-II modes never stabilize no matter how big l_m becomes is illustrated in Figs. 13 and 14. The complex values of B_l's are depicted for the HL and HF modes for $l_m=10$ and $l_m=20$. In both the high-loss and the high-frequency modes, dominant contributions come from a few modes near $l=10$ when $l_m=10$ or near $l=20$ when $l_m=20$. It is thus clear that the corresponding summation for the spatial mode function will not converge as l_m tends to infinity.

We contend that the type-I modes represent the only real physical solutions. We argue as follows.

One common property of all the type-II modes is that the amplitude of their eigenvalue λ_k tends to infinity as l_m tends to infinity. Necessarily, they must have infinite real parts and/or infinite imaginary parts. When the imaginary part of the eigenvalue is very large, the eigenvalue is discarded on the grounds that the threshold is too unrealisti-

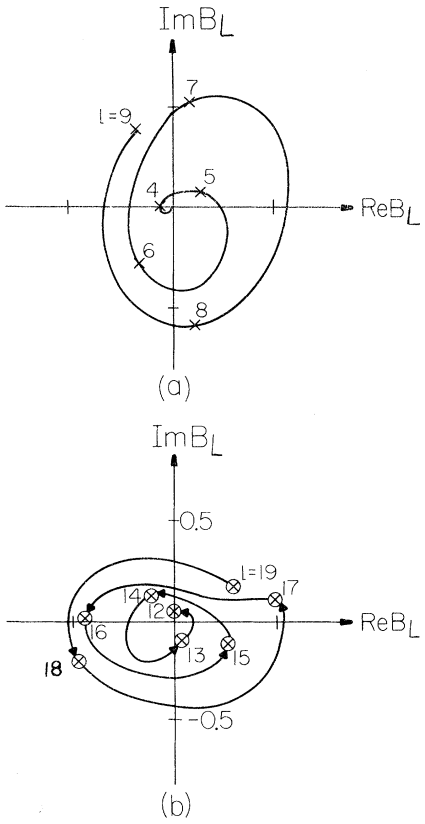

FIG. 13. Components $\{B_l\}$ for the HL mode are shown in the complex plane for $F^{-1}=1$ and for (a) $l_m=10$, (b) $l_m=20$.

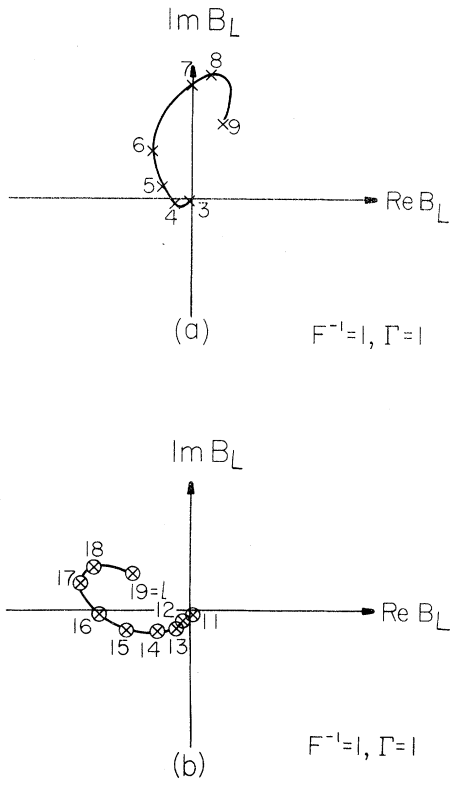

FIG. 14. Components $\{B_l\}$ for the HF mode are shown in the complex B-plane for $F^{-1}=1$ and for (a) $l_m=10$, (b) $l_m=20$.

cally high ever to excite them into lasing. When the real part is too big, its mode frequency is too far off the resonant center frequency ω_0 for it to lase.

So far, we have been concentrating on the marginally stable case $F=1$. In fact, the same discussion applies as well to any unstable case with $0<F<1$. For example, eigenvalues are plotted in Fig. 6(c) for $F=0.5$. Again, two distinct types of modes are observed. Type-I modes still have eigenvalues close to the origin. Although the relative positions of the type-II eigenvalues seem to shift to the left as a whole, the condition that

$$|\lambda_k| \to \infty \quad \text{as } l_m \to \infty$$

for these modes still prevails. Plots similar to Figs. 11–14 could be drawn also for $F=0.5$ and would show essentially the same features. They represent unphysical ill-defined solutions and will again be discarded.

We draw in Figs. 15 and 16 the amplitude plots of the field distribution for the case $F=0.5$ in the same manner as in Figs. 7 and 8. The lowest- and

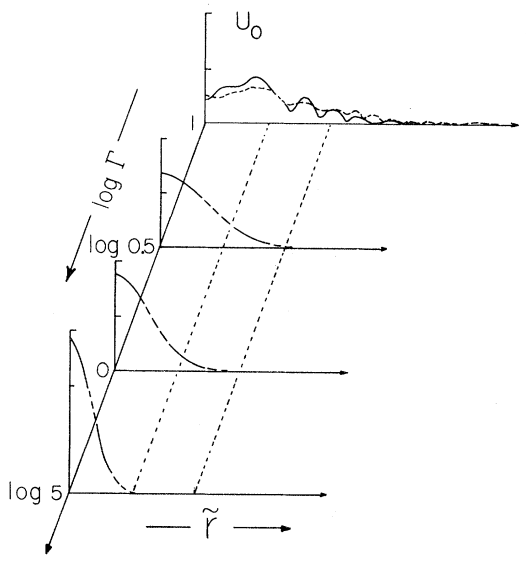

FIG. 15. Lowest-order mode pattern for the unstable case $F^{-1}=2$ with $\Gamma=0.5$, 1, 5.

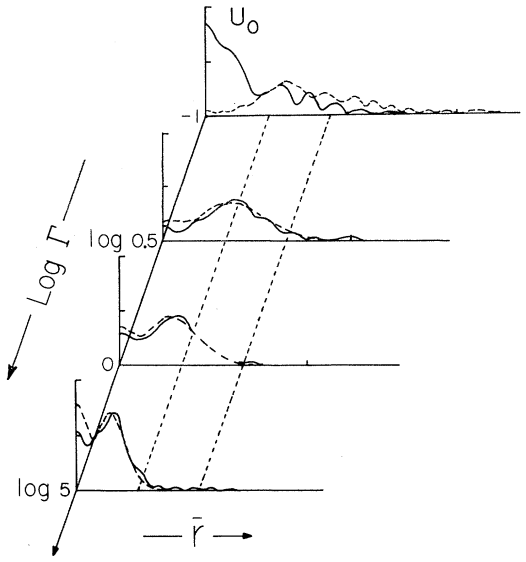

FIG. 16. Next to the lowest-order mode pattern for the unstable case $F^{-1}=2$, with $\Gamma=0.5$, 1, 5.

next-to-lowest-order type-I modes show essentially the same features as in the case $F=1$.

VIII. ASYMPTOTIC THEORY OF STRONG COUPLING

In this section we obtain analytic solutions in the asymptotic limit of $l\to\infty$ and λ small and finite. These solutions are in excellent agreement with the previous numerical calculations. This should not be unexpected for the following reasons.

Our resonator is tuned so that its symmetric q_0 mode is in resonance with the active medium, i.e., $\omega_0=\Omega_D(q_0+1)$. The most important modes in the combined lens-resonator system so far as lasing is concerned are those which have low losses and whose frequencies are near ω_0. These are just the type-I modes discussed earlier whose eigenvalues λ are small. The existence of such modes is expected in the unstable region when loss is included. The loss increases in the radial direction and tends to compensate the divergent effects due to the concave lens and thus confine the low-loss modes near the axis.

We have shown earlier in the geometrical optics limiting case ($F^{-1}\to\infty$), that the "effective optical path" parallel to the z axis increases monotonically as r^2 as we move away from the axis. We therefore expect that low-loss modes which are confined near the axis will have frequencies close to ω_0, whereas modes far from the axis will have frequencies too far from ω_0 to lase.

The numerical results of Sec. VII, especially the complex plots shown in Fig. 6, further confirm our plausibility argument. The type-I modes have small absolute values of λ_k and are well defined.

For these reasons it is not surprising that the following analytic solutions we obtain in the asymptotic limit are in very good agreement with more exact numerical results.

A. Asymptotic condition and lowest-order mode

In the present paper our approach is to construct unstable (as well as stable) resonator solutions as mixings of well-known stable resonator modes, as given in (4.3) when λ^k is complex. For well-defined physical solutions, it is necessary that the series

$$U_k(r)=\sum_0^\infty B_l^k\phi_l(s) \tag{8.1}$$

converge. A necessary condition for convergence is that

$$|B_l^k|\to 0 \quad \text{as } l\to\infty . \tag{8.2}$$

The B_l^k obey the difference eigenvalue equation

$$(-\lambda+l)B_l=(4F)^{-1}(1+i\Gamma)[(2l+1)B_l-(l+1)B_{l+1}-lB_{l-1}] . \tag{8.3}$$

Since we are obviously interested only in physical solutions, the corresponding eigenvalues λ_k must all be finite. Therefore for large enough values of l we may neglect λ. The asymptotic conditions are

$$l\gg 1, \quad l\gg|\lambda_k| . \tag{8.4}$$

To avoid confusion, since the B_l^k's which satisfy (8.3) will be independent of λ and therefore of any particular mode k, we let

$$B_l^k\to C_l \quad \text{as } l\to\infty . \tag{8.5}$$

(For a given F and Γ, all modes have same asymptotic behavior.) In this limit, (8.3) reduces to the simple difference equation

$$\beta C_l=\tfrac{1}{2}(C_{l-1}+C_{l+1}) \tag{8.6}$$

as $l\gg 1$, where

$$\beta\equiv(\beta'+i\Gamma)/(1+i\Gamma) \tag{8.7}$$

and

$$\beta'=1-2F . \tag{8.8}$$

In terms of β', the stability conditions now become

Stable: $\begin{cases}\beta' > 1 & \text{convex lens}(F<0)\ ,\\ \beta' < -1 & \text{concave lens}\ (F>0)\ ,\end{cases}$

Unstable: $-1<\beta'<-1$, (8.9)

Marginally stable: $\beta' = -1$,

Severly unstable limit: $\beta' = 1$.

To solve (8.6), we let

$$C_l = C_0\eta^l \equiv C_0 \exp[(-1/l' + i2\pi/p')l] \tag{8.10}$$

in (8.6). Thus, we obtain the two solutions

$$\eta_\pm = \beta \pm (\beta^2 - 1)^{1/2} \ . \tag{8.11}$$

By (8.2), the physical solution requires that

$$|C_l| \to 0 \ \text{ as } l \to \infty \ . \tag{8.12}$$

By (8.10) and (8.11), this requires that[16] the choice of $\eta_\pm$ is determined by

$$|\eta| < 1 \tag{8.13}$$

or

$$l' = -1/\mathrm{Re}(\ln\eta) > 0 \ . \tag{8.14}$$

B. Field amplitude in asymptotic limit

In the limit of large l and finite small λ's, the field amplitude (8.1) becomes in this limiting case

$$U(r) = \sum_0^\infty C_l\phi_l(s) = C_0 e^{-s/2}\sum_0^\infty \eta^l L_l(s)$$
$$= C_0 e^{-s/2}\sum_0^\infty e^{-l/l'}e^{i2\pi l/p'}L_l(s) \ . \tag{8.15}$$

We have used (3.42) and (8.10). Since $l' > 0$ for physical solutions, we see that modes for which $l > l'$ do not contribute much to the field amplitude. Thus l' is the effective number of stable modes needed to describe the asymptotic field, $l' \sim l_{\text{eff}}$. Since $|\eta| < 1$, the series in (8.15) may be summed, if we use the well-known generating function for Laguerre polynomials.[12] Thus,

$$U(r) = [C_0/(1-\eta)]\, e^{-s/2}e^{s\,\eta/(\eta-1)}$$
$$= [C_0/(1-\eta)]\, e^{-r^2/w'^2} \ , \tag{8.16}$$

where

$$w'^2/w_0^2 \equiv (1-\eta)/(1+\eta) \ . \tag{8.17}$$

The field is therefore seen to be quasi-Gaussian with w'^2 as the complex effective beam width. From this and (8.10) we have that

$$\left(\frac{w_0}{w'}\right)^2 \equiv \left(\frac{w_0}{w_r}\right)^2 + i\left(\frac{w_0}{w_i}\right)^2 = \frac{1+\eta}{1-\eta}$$
$$= \frac{1 - e^{-2/l'} + 2ie^{-1/l'}\sin(2\pi/p')}{1 + e^{-2/l'} - e^{-1/l'}2\cos(2\pi/p')} \ . \tag{8.18}$$

Since the lowest-order mode has the smallest eigenvalue, we expect that (8.16) will be a good approximation to the lowest-order mode. We may obtain its eigenvalue as follows.

If we let

$$B_l = B_0\eta^l \tag{8.19}$$

in (8.3) and sum both sides over all l, we obtain

$$\lambda = \frac{\sum_{l=0}^\infty l\eta^l - (4F)^{-1}(1+i\Gamma)\eta^{-1}\sum_{l=0}^\infty [(2l+1)\eta - (l+1)\eta^2 - l]\eta^l}{\sum_{l=0}^\infty \eta^l} \ . \tag{8.20}$$

Since $|\eta| < 1$, all terms may be summed exactly so that we find after minor algebra that

$$\lambda_0 = \eta/(1-\eta) \ . \tag{8.21}$$

The mode frequency is thus

$$\Omega_0 = \omega_0 + \theta\Omega_D\,\mathrm{Re}[\eta/(1-\eta)] \tag{8.22}$$

and the corresponding linewidth is

$$\gamma_0 = -\theta\Omega_D\,\mathrm{Im}[\eta/(1-\eta)] \ . \tag{8.23}$$

We proceed to study several special cases.

1. *No loss* ($\Gamma = 0$)

When $\Gamma = 0$, we have by (8.7) and (8.8)

$$\beta \to \beta' = 1 - 2F \ , \tag{8.24}$$

while by (8.11)

$$\eta_\pm = \beta' \pm (\beta'^2 - 1)^{1/2} \ . \tag{8.25}$$

The unstable region, by (8.9), corresponds to $\beta'^2 < 1$. In this event

$$\eta_\pm = \beta' \pm i(1-\beta'^2)^{1/2} \ , \tag{8.26}$$

so that

$$|\eta_\pm| = 1 \ . \tag{8.27}$$

However, for physical solutions to exist, by (8.13), $|\eta| < 1$. We conclude that when no loss is present, no physical solutions exist in the unstable region.

In particular, the severely unstable limit yields, with $\beta' = 1 (F^{-1} \to \infty)$,

$$\eta = 1 \ , \tag{8.28}$$

and the asymptotic expansion for the field (8.15) becomes

$$U(r) = C_0 e^{-s/2}\sum_{l=0}^\infty L_l(s) = C_0\delta(s) \ , \tag{8.29}$$

which is the same as the lowest-order mode $r' = 0$

of Eq. (4.15) obtained previously.

For the marginally stable case $\beta' = -1$ (i.e., $F^{-1} = 1$), the field (8.15) becomes

$$U(r) = C_0 e^{-s/2} \sum_{l=0}^{\infty} (-1)^l L_l(s) \ . \tag{8.30}$$

From the generating function

$$\sum_{l=0}^{\infty} y^l L_l(s) = (1-y)^{-1} e^{sy/(y-1)} \ , \tag{8.31}$$

if we let $y = -1 + \epsilon$, we have for $\epsilon \ll 1$

$$\sum_{l=0}^{\infty} (-1)^l L_l(s) = \tfrac{1}{2} e^{s/2} \ . \tag{8.32}$$

Thus,

$$U(r) \to \text{const.} \tag{8.33}$$

The numerical solutions of Sec. V show that the lowest-order Gaussian mode does flatten out as the transition point ($F^{-1} = 1$) is approached. The trend, as seen from the $l_m = 10$, 20, and 40 results, points toward uniformity over all space as $l_m \to \infty$, in agreement with (8.23).

Let us study the field as we approach the transition region from the stable side. We therefore let

$$\beta' = -1 - \epsilon \ , \tag{8.34}$$

where ϵ is small and positive. Then, by (8.25) we have

$$\eta = \eta_+ = \beta' + (\beta'^2 - 1)^{1/2} \cong -1 + (2\epsilon)^{1/2} + \theta(\epsilon) \tag{8.35}$$

for the physically real mode. We may write this as

$$\eta = -e^{-1/l'} \ , \tag{8.36}$$

where the "correlation length" l' is

$$l' = 1/(2\epsilon)^{1/2} \tag{8.37}$$

and it diverges as we approach the transition region ($\epsilon \to 0$).

The field (8.16) then yields the asymptotic distribution

$$U(r) \sim C_0/2e^{-r^2/w_r^2} \tag{8.38}$$

where by (8.18)

$$(w_r/w_0)^2 = 2l' = (2/\epsilon)^{1/2} \ . \tag{8.39}$$

The numerical results shown in Fig. 4 indicate the onset of such behavior. The lack of complete agreement is limited by the finite l_m used in the computations. The beam width becomes very broad in agreement with experiment.

2. *Marginally stable case with loss*

Let us consider the large Fresnel number limit in which $N_F \gg 1$, which by (6.10) corresponds to small loss Γ. When $F^{-1} = 1$, by (8.8), $\beta' = -1$. When $\Gamma \ll 1$, we have by (8.7)

$$\beta = -(1 - i\Gamma)/(1 + i\Gamma) \tag{8.40}$$

and by (8.11)

$$\eta_\pm \cong -1 \pm (2\Gamma)^{1/2} \pm i(2\Gamma)^{1/2} + O(\Gamma) \ . \tag{8.41}$$

The condition (8.13) demands η_- be discarded. Thus,

$$\eta = \eta_+ = -e^{-(1/l')(1-i)} \ , \tag{8.42}$$

where

$$1/l' = 2\pi/p' = (2\Gamma)^{1/2} \ . \tag{8.43}$$

The asymptotic field distribution (8.16) becomes

$$U(r) \cong C_0/2e^{-r^2/w'^2} \ , \tag{8.44}$$

where the effective beam width is by (8.18)

$$(w_r/w_0)^2 = 2l' = (2\Gamma)^{1/2} = -(w_i/w_0)^2 \ . \tag{8.45}$$

If we compare (8.44) with the numerical results shown in Fig. 7, we see that this asymptotic solution describes the lowest-order mode very well indeed. First of all, the Gaussian amplitude dependence is apparent for all Γ. Secondly, the width narrows as Γ increases as seen in Fig. 7. This trend is predicted by (8.45), although it was derived for small Γ.

It is interesting to point out that although the number of modes coupled in the numerical solutions is not large ($l_m = 10, 20, 40$), the features of the lowest-order mode agree well with the asymptotic predictions.

We may estimate the amount of loss needed in the numerical calculations in order for the type-I modes to stabilize when l_m is fixed. We require that

$$l' \ll l_m \ ,$$

which by (8.33) requires that

$$\Gamma \gg 1/2l_m^2 \ ,$$

or for $l_m = 10$, $\Gamma \gg 5 \times 10^{-3}$.

The generalization for arbitrary Γ is straightforward. For simplicity, we consider only the case of $\Gamma = 1$.

With $F^{-1} = 1$ and $\Gamma = 1$, we have that $\beta' = -1$, $\beta = i$. Thus,

$$\eta = \eta_+ = e^{-i\pi/2} e^{-1/l'} \ , \tag{8.46}$$

where

$$l' = -[\ln(\sqrt{2} - 1)^{1/2}]^{-1} \ . \tag{8.47}$$

Thus, according to (8.10)

$$C_l = C_0 e^{-l/l'} e^{-i(\pi/2)l} \ . \tag{8.48}$$

This is in agreement with Fig. 9, which shows a monotonic decrease of the modulus of the successive complex vectors B_l^0 as we increase l and the rotation in steps of $-\frac{1}{2}\pi$ of the phase.

3. *Limit of large Fresnel number*

We next consider the general asymptotic solutions in the entire unstable range $(-1< \beta'< 1)$ when $\Gamma \ll 1$.

For small Γ, by (8.7) we have

$$\beta=(\beta'+i\Gamma)/(1+i\Gamma), \tag{8.49}$$

so that by (8.11)

$$\eta_{\pm}\cong\left[1\pm\Gamma\left(\frac{1-\beta'}{1+\beta'}\right)^{1/2}\right][\beta'\pm i(1-\beta'^2)^{1/2}]. \tag{8.50}$$

This is valid if

$$\Gamma\ll|1+\beta'|. \tag{8.51}$$

Notice that this condition cannot be satisfied when $\beta'=-1$. Since $|\eta_{\pm}|\cong 1\pm\Gamma[(1-\beta')(1+\beta')]^{1/2}$, we must discard η_+ and take

$$\eta=\eta_-=e^{-1/l'}e^{i2\pi/p'}, \tag{8.52}$$

where

$$\begin{aligned} l'&\cong\Gamma^{-1}[(1+\beta')/(1-\beta')]^{1/2},\\ 2\pi/p'&=-\tan^{-1}[(1-\beta'^2)^{1/2}/\beta'] \end{aligned} \tag{8.53}$$

and $\beta'\neq -1$.

The asymptotic field pattern (8.16) becomes

$$U_r=[C_0/(1-\eta)]\,e^{-(1/w_r'^2+i/w_i'^2)r^2} \tag{8.54}$$

where by (8.18)

$$(w_r/w_0)^2\cong l'[1-\cos(2\pi/p')] \tag{8.55}$$

and

$$\left(\frac{w_i}{w_0}\right)^2\cong\frac{1-\cos(2\pi/p')}{\sin(2\pi/p')}. \tag{8.56}$$

We have used the fact that $l'\gg 1$, which follows from (8.53). Thus, the beam width is large compared with w_0 in agreement with experiment.

We consider first the limit $\beta'=-1+\epsilon'$, where $\epsilon'\to 0^+$. To be consistent with (8.51), we also require that

$$\Gamma\ll\epsilon'. \tag{8.57}$$

By Eqs. (8.53)–(8.56), we see that the correlation length l' and the beam width decrease as transition point is approached. On the other hand, the pitch p' and w_i' increase. That is, as $\epsilon'\to 0$, $\epsilon'\gg\Gamma$:

$$\begin{aligned} &l'\to\Gamma^{-1}(\epsilon'/2)^{1/2},\quad 2\pi/p'\to(2\epsilon')^{1/2}+\pi,\\ &(w_r/w_0)^2\to(2\epsilon')^{1/2}/\Gamma,\quad (w_i/w_0)^2\to(2/\epsilon')^{1/2}. \end{aligned} \tag{8.58}$$

In the strong-coupling limit, $\beta'=1-\epsilon_\infty$, where $\epsilon_\infty\to 0^+$. Then

$$\begin{aligned} &l'\sim\Gamma^{-1}(2/\epsilon_\infty)^{1/2},\quad 2\pi/p'-(2\epsilon_\infty)^{1/2},\\ &(w_r/w_0)^2\sim\Gamma^{-1}(2\epsilon_\infty)^{1/2},\quad (w_i/w_0)^2\sim-(\epsilon_\infty/2)^{1/2}. \end{aligned} \tag{8.59}$$

Again, we see l' is very large.

C. Higher-order modes in asymptotic limit

It is relevant for mode control considerations in practical problems to determine the frequences as well as the decay constants for other low-order modes. We need to pursue the theory beyond the lowest order.[17] For this purpose, let us consider solutions of (8.3) of the form

$$\begin{aligned} B_l&=Bb_l\eta^l\\ &\equiv Bb_l\,e^{(-1/l'+2\pi/p')l}. \end{aligned} \tag{8.60}$$

If we use this in (8.3), we obtain

$$[\Lambda+1+2\beta l]b_l+lb_{l-1}\eta^{-1}+(l+1)\eta b_{l+1}=0, \tag{8.61}$$

where

$$\Lambda=4F\lambda/(1+i\Gamma) \tag{8.62}$$

and β is given by (8.7).

For simplicity let us only consider the low-loss case $\Gamma\ll 1$ near the transition point for which

$$\beta'=-1+\epsilon', \tag{8.63}$$

where $\epsilon'\to 0^+$ and $\Gamma\ll\epsilon'$. In this case, we have by (8.58)

$$\eta\cong-e^{-\delta}, \tag{8.64}$$

where

$$\begin{aligned} \delta&=1/l'-i[(2\pi/p')-\pi]\\ &=\Gamma(2/\epsilon')^{1/2}-i(2\epsilon')^{1/2}\ll 1, \end{aligned} \tag{8.65}$$

since $\Gamma\ll\epsilon'$. Also

$$\beta=(\beta'+i\Gamma)/(1+i\Gamma)\approx-1. \tag{8.66}$$

Therefore, (8.61) becomes

$$(\Lambda+1-2l)b_l+lb_{l-1}[1-\delta]+(l+1)b_{l+1}[1+\delta]\cong 0. \tag{8.67}$$

As $l\to\infty$, we have

$$B_l\to\eta^l=-e^{-\delta l}, \tag{8.68}$$

so by (8.60)

$$b_l\eta^l\to\text{const}. \tag{8.69}$$

We are interested in the limiting case in which $l\to\infty$, $\delta\to 0$, so that

$$y=l\delta \tag{8.70}$$

becomes a continuous variable. Also

$$b_l \to b(y), \quad b_{l\pm1} \to b(y\pm\delta); \tag{8.71}$$

and we assume $b(y)$ is slowly varying:

$$(\delta\, d/dy)^n b(y) \gg (\delta\, d/dy)^{n+1} b(y)\,. \tag{8.72}$$

In this way, we convert the difference equation (8.67) to the differential equation

$$y\frac{d^2b}{dy^2} + (1-2y)\frac{db}{dy} + \frac{\Lambda+2-\delta}{\delta}\,b = 0 \tag{8.73}$$

for terms of lowest order in δ. We have expanded $b(y\pm\delta)$ by a Taylor series up to second order. If we let $u=2y$, this is the confluent hypergeometric equation.[18] The solution which is finite for $y=0$ is

$$b(y) = C_1 F_1(a; b; 2y), \tag{8.74}$$

where

$$a = -(\Lambda+2-\delta)/2\delta, \quad b = 1\,. \tag{8.75}$$

For $y\to\infty$, by (8.68)–(8.71), we have

$$b(y)e^{-y} \to \text{const.} \tag{8.76}$$

Since[18]

$$e_1^{-y}F_1(a; b; 2y) \xrightarrow[y\to\infty]{} \frac{\Gamma(b)}{\Gamma(b-a)}\,e^{\pi a}e^{-y}y^{-a} + \frac{\Gamma(b)}{\Gamma(a)}\,y^{a-b}\,. \tag{8.77}$$

We can satisfy (8.66) if $\Gamma(a)=\infty$ or

$$a = -k, \tag{8.78}$$

where k is an integer. In this case, $b(y)$ reduces to Laguerre polynomials. By (8.75) and (8.76), we obtain the eigenvalues

$$\Lambda_k = -2+\delta(2k+1) = 4F\lambda_k/(1+i\Gamma), \tag{8.79}$$

where we used (8.62). The mode eigenfrequencies are

$$\begin{aligned}\Omega_k &= \omega_0 + \Omega_D\,\theta\,\mathrm{Re}\lambda_k \\ &\cong \omega_0 + \Omega_D\,\theta[-\tfrac{1}{2} + (2k+1)\,\Gamma(2/\epsilon')^{1/2}/4],\end{aligned} \tag{8.80}$$

since $F^{-1}\approx+1$. The mode linewidth is

$$\begin{aligned}\gamma_k &= -\Omega_D\,\theta\,\mathrm{Im}\lambda_k \\ &\approx \Omega_D\,\theta(2k+1)\,(2\epsilon')^{1/2}/4\,.\end{aligned} \tag{8.81}$$

It is interesting to note that the linewidth is independent of the loss Γ and the Fresnel number N_F. This is consistent with the geometrical optics arguments of Siegman.[1]

It is also interesting to point out that the lowest eigenvalue obtained in (8.11),

$$\lambda = \eta/(1-\eta), \tag{8.82}$$

agrees with (8.80) and (8.81) for $k=0$. This is seen if we use (8.64) and (8.65) with $\delta \ll 1$.

IX. SUMMARY

Unlike much of the previous work on unstable resonator systems, the effects of the active lasing medium may be naturally included in our approach, and will be treated in detail in a forthcoming paper. In the present paper we concentrate on properties of the unstable resonator from our multimode approach.

Symmetry considerations enable us to reduce a complicated three-dimensional problem to a much simpler one-dimensional linear-chain problem, which we are able to solve analytically in the asymptotic limit. Our asymptotic theory predicts the behavior of the lowest-loss resonant modes in unstable resonators and is supported by numerical computations.

In the stable-unstable transition region, as well as in the entire unstable region, the lowest-order mode pattern retains its Gaussian form when the losses are included (to account for finite mirrors) in the model. Without losses, the beam width diverges as the transition point ($F^{-1}=1$) is approached from the stable region as indicated by Eq. (8.39). With the loss included, the beam width will be finite. For small fixed losses, it decreases as the transition point is approached from the un-

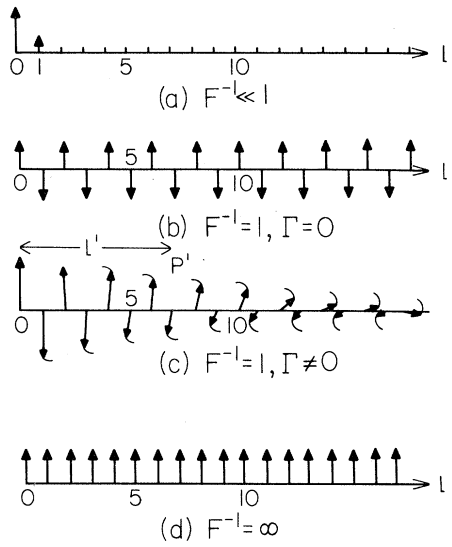

FIG. 17. Pictorial representations of the asymptotic solutions in different regions of stability: (a) Stable region with $|F^{-1}|\ll 1$. Short-range order prevails. (b) Marginal case without loss ($F^{-1}=1$, $\Gamma=0$). Antiferromagnetic type of order occurs. (c) Marginal case with loss ($F^{-1}=1$, $\Gamma\neq 0$). The effects of the loss are twofold: One is to render the correlation length l' finite; the other is to cause a twist with pitch P'. (d) Strong-coupling limit $F^{-1}\to\infty$. Ferromagnetic type of ordering results.

stable side as shown in Eq. (8.58). It again decreases towards severely unstable region as illustrated by the strong-coupling result of Eq. (8.59).

We find the following physical picture for what happens when a resonator goes unstable useful (see Fig. 17).

We regard the modes in any resonator, stable or unstable, as mixings of the well-known modes in some appropriately chosen stable resonator, each of which is represented by a fixed site, equally spaced on a straight line. The complex mixing coefficient (B_l^k) of the mode is represented by a "spin" on that site, free to rotate in the plane perpendicular to the line when the interaction is turned off ($F^{-1}=0$). When the interaction, which involves nearest neighbors only, is turned on, the spins will couple as in a linear chain and behave cooperatively. In the stable region, there exists only short-range order and it is described by a small correlation length. On the other hand, long-range order involving a large number of spins occurs near the transition point (marginally stable), an antiferromagnetic type of ordering, with neighboring spins aligned antiparallel, occurs. [See Eq. (8.30).] The effect of diffraction loss is to render the correlation length finite and to cause a "twist" of the spins, relative to one another, all the way down the linear chain.

In the limit of very severe instability ($F^{-1}\to\infty$), a ferromagnetic type of ordering, with all spins aligned, results [see Eq. (8.28)] and the correlation length becomes large again.

ACKNOWLEDGMENTS

The authors would like to express their thanks to Y. C. Lin for his assistance in numerical calculations, and to J. Hanlon, Y. C. Lin, and R. Shea for numerous discussions. We are also indebted to E. B. Treacy for bringing his results to our attention and for stimulating discussions.

---

*A preliminary account of this work was presented at the Third Winter Colloquium on Quantum Electronics at Alta, Utah (January 1973), and at the Conference on the Physics of Quantum Electronics at Crystal Mountain, Washington (July 1973).

†Supported by the Air Force Laser Laboratory, Kirtland AFB, N. M. 87117.

‡Permanent address: Department of Physics and Electrical Engineering, University of Southern California, Los Angeles, Calif. 90007.

[1]A. E. Siegman, Proc. IEEE 53, 277 (1965); A. E. Siegman and R. Arrathoon, IEEE J. Quant. Electron. QE-3, 156 (1967).

[2]S. Barone, Appl. Opt. 6, 861 (1967).

[3]L. Bergstein, Appl. Opt. 7, 495 (1968).

[4]W. Streifer, IEEE QE-4, 229 (1968).

[5]A. Fox and T. Li, (a) Proc. IEEE S-1, 80 (1963); *Quantum Electronics III* (Columbia U. P., New York, 1964), p. 1263.

[6]R. Sanderson and H. Streifer, (a) Appl. Opt. 8, 131 (1969); (b) Appl. Opt. 8, 2129 (1969).

[7]W. Lamb, Jr., Phys. Rev. 134, A1429 (1964).

[8]Numerical calculations including the effects of gain were presented by A. E. Siegman and E. Sziklas at the Third Winter Conference on Quantum Electronics at Alta, Utah (January 1973) and at the Fourth Conference at Aspen, Colorado (January 1974). Analytical solutions have been obtained by E. B. Treacy, Report No. L920936-5, United Aircraft Research Labs, 1972 (unpublished).

[9]R. Lang, M. O. Scully, and W. E. Lamb, Jr., Phys. Rev. A 7, 1788 (1973).

[10]H. Kogelnik and T. Li, Appl. Opt. 5, 1550 (1966).

[11]It is well known that the stable cavity modes we use (Ref. 10) are not rigorously orthogonal or complete. However, they are derived from Maxwell's equations after making a paraxial approximation. It can be shown that within the accuracy of the paraxial approximation, they are approximately orthogonal. The nonorthogonal contribution represents a correction of order $(k_{q'l'm'}-k_{qlm})/k_{qlm}$, which is extremely small for typical resonators. It may also be noted that in carrying out the orthogonality integral, one must first do the radial integration for a fixed z such that one does not "hit" the mirror. This has the effect of limiting the number of "modes" for a given Fresnel number so that they are not rigorously complete.

[12]I. Gradshteyn and I. Ryzhik, *Table of Integrals, Series, and Products* (Academic, New York, 1965).

[13]See, for example, B. Rossi, *Optics* (Addison-Wesley, Reading, Mass., 1957), p. 84.

[14]A light beam, confined to a region of space with transverse dimension a_{eff}, has its first diffraction maximum at an angle $\theta_d\cong\lambda/a_{\text{eff}}$. The spread in the transverse direction, therefore, is $\Delta\cong D\theta_d=\lambda D/a_{\text{eff}}$, after the beam has traveled a distance D. The Fresnel number is defined as the ratio Δ/a_{eff}.

[15]The discussion here applies in fact to any finite value of Γ. For smaller values of Γ, type-I eigenvalues will exist for larger values of $l_{\max}$ than what we obtained in our numerical solutions.

[16]Since the assumed solution (8.10) implies an asymptotic power series, the condition (8.13) is therefore both necessary and sufficient for the series in (8.1) to converge.

[17]Using a different approach, Treacy has also obtained solutions similar to ours (Ref. 8). Comparison with his and others' results will be discussed elsewhere.

[18]M. Abramowitz and I. Stegun, *Handbook of Mathematical Function* (Dover, New York, 1965).